Steady-state expansion of current-carrying plasma into vacuum

I. A. Krinberg, M. P. Lukovnikova, and V. L. Papernyĭ

Irkutsk State University
(Submitted 26 July 1989; resubmitted 4 November 1989)
Zh. Eksp. Teor. Fiz. **97**, 806–820 (March 1990)

The steady-state spherical expansion of a current-carrying plasma into vacuum is studied in the hydrodynamic approximation. The plasma can become supersonic at one value of a characteristic parameter of the flow. In this case the spatial variation of the hydrodynamic properties of the plasma is determined unambiguously by the integral electron and ion fluxes from a spherical surface of a given radius and can be calculated without specifying boundary conditions on this surface. A quantitative interpretation based on this theory for spherical expansion of a plasma is offered for the existing extensive experimental data on vacuum arcs.

INTRODUCTION

A detailed theory has now been derived for both the steady-state expansion[1-3] and the time-varying expansion[4-6] of a current-free plasma, in the case in which ions are accelerated by the ambipolar electric field which arises because the electrons move ahead of the ions. Also of substantial interest is the expansion of current-carrying plasma jets which are directed opposite a current flow. A situation of this type arises in vacuum arcs,[7-9] in the upward-directed, current-carrying fluxes of O^+ which are formed in certain regions of the space environment of the earth,[10] and (apparently) in certain parts of the solar corona.

The literature reveals no study of the steady-state expansion of a current-carrying plasma in a general formulation of the problem. Steady-state hydrodynamic equations were solved in Refs. 11–15 for a vacuum arc for certain particular values of the initial parameters of the problem, through the use of boundary conditions on a surface from which plasma is flowing. As a result, the solutions which were found were largely determined by these conditions. Furthermore, those papers ignored the effect of the electron thermal conductivity on the expansion process.

Our purposes in the present study were to construct a solution for the problem in the general case, to analyze the behavior of the resulting solution as a function of the initial parameters of the problem, and to study the effect of thermal conductivity. We use the solution found here to analyze the extensive existing experimental data on current-carrying plasma jets in vacuum arcs.

1. SYSTEM OF EQUATIONS

We consider a fully ionized plasma consisting of electrons (with a temperature T_e) and cold ions ($T_i = 0$) with an arbitrary charge $Z_i e$. Previous calculations[3,4] have shown that the thermal spread of the ions has little effect on the solution for an expanding current-free plasma, because of the low thermal conductivity of the ions and their rapid cooling during the plasma expansion. The approximation $T_i = 0$ rests on an even firmer basis in the case of a current-carrying plasma (as is demonstrated by the results calculated in Ref. 14), in which case there is a heating of electrons.

We begin by writing hydrodynamic equations for a plasma jet, making use of the steady-state nature of the process. The continuity equations for the electrons and ions are

$$eN_eV_eS=I_e, \quad Z_ieN_iV_iS=I_i, \tag{1}$$

where N_e and N_i are the electron and ion densities, V_e and V_i are their average velocities, S is the cross-sectional area of the jet, and I_e and I_i are the electron and ion currents ($I_e - I_i = I$ is the current in the jet).

The equations of motion of the electrons and ions along the jet axis reduce to the following form if we ignore the electron inertia and the viscosity:

$$0 = -\frac{d(N_eT_e)}{dr} + eN_e\frac{d\Phi}{dr} - R, \tag{2}$$

$$m_iN_iV_i\frac{dV_i}{dr} = -Z_ieN_i\frac{d\Phi}{dr} + R, \tag{3}$$

where m_i is the ion mass, and Φ is the electric potential. The transfer of momentum from electrons to ions is determined by the equation[16,17]

$$R = -\frac{eN_e}{\sigma}j + \alpha_T N_e\frac{dT_e}{dr}, \tag{4}$$

where $j = e(Z_iN_iV_i - N_eV_e) = -I/S$ is the current density; $\sigma = Z_ie^2/m_e v_e\sigma_{ei}$ is the electrical conductivity; $v_e = (2T_e/m_e)^{1/2}$; $\sigma_{ei} = \delta Z_i^2 e^4 \ln\Lambda/T_e^2$ is the effective cross section of the Coulomb interaction; and α_T is the coefficient for the thermoforce (at $Z_i = 1$ we have $\alpha_T = 0.7$ and $\delta = 1.2$; at $Z_i = 2$ we have $\alpha_T = 0.9$ and $\delta = 1.0$; and at $Z_i = 3$ we have $\alpha_T = 1.0$ and $\delta = 0.9$).

The energy balance equation for the overall plasma can be written as follows (where we are using $\nabla j = 0$ and $m_iV_i^2 \gg m_eV_e^2$):

$$\left(q_e - \alpha_T T_e j/e + \frac{5}{2}T_eN_eV_e + \frac{m_iV_i^2}{2}N_iV_i + j\Phi\right)S = H. \tag{5}$$

Here $q_e = -\varkappa_e(dT_e/dr)$ is the heat flux, $\varkappa_e = \varepsilon_\varkappa\sigma T_e/e^2$ is the thermal conductivity (for $Z_i = 1, 2,$ and 3 we have $\varepsilon_\varkappa = 1.61, 2.15,$ and 2.44, respectively),[16,17] and H is a constant of the flow.

Instead of the Poisson equation for the potential we will use the quasineutrality condition $N_e = Z_iN_i$; along with this condition, Eqs. (1)–(3) and (5) constitute a complete system of equations.

Since we have $\gamma = I_e/I_i = V_e/V_i = $ const under quasineutrality conditions (the case $\gamma = 1$ corresponds to a current-free plasma), we can use Eq. (1) to eliminate the particle density and the velocity V_e. The system of equations then reduces to three equations in the unknowns V_i, T_e, and Φ

(we will be replacing the velocity V_i by the ion energy $W_i = m_i V_i^2/2$).

We choose some point $r = r_*$ (an arbitrary point for the time being), and we denote the values of the properties at this point by $N_i = N_*$, $W_i = W_*$, $T_e = T_*$, $\Phi = \Phi_*$, and $S = S_*$. We then transform to dimensionless variables $x = r/r_*$, $n = N_i/N_*$, $w = W_i/W_*$, $t = T_e/T_*$, $\varphi = \Phi/\Phi_*$, $s = S/S_*$, so that at $x = 1$ we now have $n = w = t = s = 1$. Since the origin of the scale can be put anywhere, we set $\Phi_* = T_*$ at the point $r = r_*$. From Eqs. (1)–(5) we then find

$$\left(\alpha - \frac{t}{2w}\right)\frac{dw}{dx} = \frac{t}{s}\frac{ds}{dx} - \frac{dt}{dx}, \tag{6}$$

$$\frac{d}{dx}(\alpha w + \varphi - \alpha_T t) = \frac{\beta}{\varepsilon s t^{\frac{1}{2}}}, \tag{7}$$

$$\frac{\alpha}{\gamma} w + \left(\frac{5}{2} + \alpha_T \varepsilon\right) t - \varepsilon \varphi - \frac{e_* e^2}{\beta} s t^{5/2} \frac{dt}{dx} = h, \tag{8}$$

where $\alpha = W_*/Z_i T_*$, $\varepsilon = 1 - \gamma^{-1} = I/I_e$ ($0 \geqslant \varepsilon \geqslant 0$), and h is a normalized constant of the flow.

After solving Eqs. (6)–(8), we can find the particle density distribution from the algebraic relation $nw^{1/2}s = 1$.

Equations (7) and (8) contain the characteristic flow parameter

$$\beta = \frac{e\varepsilon I r_*}{\sigma_* T_* S_*} = 2\varepsilon^2 \frac{M_*}{Kn_*}, \tag{9}$$

which can be interpreted as the ratio of the Joule energy evolution $I^2/\sigma s$ to the convective heat removal (from a unit layer) $T_e N_e V_e S/r = T_e I/e\varepsilon r$ at the point $r = r_*$ [here $\sigma(T_*) = \sigma_*$]. This parameter can also be expressed in terms of the Mach number $M_* = V_{e*}/v_{e*}$ and the Knudsen number $Kn_* = \lambda_*/r_*$ for the electrons [here $\lambda_* = 1/N_* \sigma_{ei}(T_*)$ is the effective mean free path of an electron at the point $r = r_*$].

Natural conditions on expansion into vacuum are the requirements $T_e \to 0$ and $N_i \to 0$ as $r \to \infty$ (or $t \to 0$ and $n \to 0$ as $x \to \infty$). Taking these conditions into account, but not specifying boundary conditions on the surface of the source at $r = r_1$, we turn to an analysis of system of equations (6)–(8).

2. FLOW OF A NON-HEAT-CONDUCTING PLASMA

Let us consider the problem of solving system (6)–(8) under the assumption $\beta \gg 1$, under which we can ignore the last term on the left side of (8), i.e., the electron heat flux. From (6)–(8) we then find

$$\frac{dw}{dx} = \left(\frac{t}{s}\frac{ds}{dx} - \frac{2\beta}{5st^{\frac{1}{2}}}\right)\bigg/\left(\frac{3\alpha}{5} - \frac{t}{2w}\right) \tag{10}$$

$$\frac{dt}{dx} = \left[\frac{2\alpha t}{5s}\frac{ds}{dx} - \left(\alpha - \frac{t}{2w}\right)\frac{2\beta}{5st^{\frac{1}{2}}}\right]\bigg/\left(\frac{3\alpha}{5} - \frac{t}{2w}\right). \tag{11}$$

Since the experimental data describe an acceleration of ions in current-carrying jets to velocities far higher than the ion sound velocity[15,18] $V_s \approx (T_e/m_i)^{1/2}$, we restrict the discussion below to those flow conditions which result in a crossing of the sound velocity. The condition for this crossing is the simultaneous vanishing of the numerator and denominator in (10). For a monotonically increasing cross-sectional area of the jet ($ds/dx < 0$), we see in particular

from (9) and (10) that a transition to supersonic flow is not possible for the steady-state current-flow expansion ($\gamma = 1$, $\varepsilon = \beta = 0$) of a non-heat-conducting plasma. A transition to a supersonic flow does become possible if there is a current ($\gamma > 1$, $\beta \neq 0$). We will examine this possibility in more detail for the spherical expansion of a plasma, with $s(x) = x^2$.

We assume that the critical cross section, at which the numerator and denominator in (10) vanish simultaneously, is at the point $r = r_*$, i.e., at $x = 1$. For this point we then have $t = w = 1$, and from (10) we find $\alpha = 5/6$ and $\beta = 5$. Substituting these values into (10) and (11), we find

$$\frac{dw}{dx} = \frac{4t}{x}\frac{1 - 1/xt^{5/2}}{1 - t/w} \tag{12}$$

$$\frac{dt}{dx} = -\frac{2t}{3x}\frac{2 - (5 - 3t/w)/xt^{5/2}}{1 - t/w}. \tag{13}$$

We see that Eqs. (12) and (13) contain no parameters of the flow at all. Consequently, their solution $w(x)$ and $t(x)$ (derived under the boundary condition $w = t = 1$ at $x = 1$) will be universal functions. Making use of the same boundary condition, we find the value of the flow from Eq. (8):

$$h = \frac{5}{6\gamma} + \frac{5}{2} + (\alpha_T - 1)\varepsilon.$$

For the values found for the parameters α and β, the derivatives $dw/dx = w'_*$ and $dt/dx = t'_*$ are indeterminate at the critical point, $x = 1$. Using L'Hôpital's rule, we find from (12) and (13) the algebraic equations

$$w'_*(w'_* - t'_*) = 10t'_* + 4, \quad w'_* = 3(2 - t'_*). \tag{14}$$

Solving them, we find $w'_* \approx 3.75$ and $t'_* \approx 0.75$. Using these values, we can carry out a numerical integration of Eqs. (12) and (13) in both directions away from the critical point. The solution found is shown by the dot-dashed line in Fig. 1.

The procedure for finding a solution [an integration of Eqs. (12) and (13) from the point $x = 1$ into the region $x < 1$] shows that there exists a unique supersonic solution $w(x)$, $t(x)$, whose form does not depend on the boundary conditions. The relative radius of the source, in this case $x_1 = r_1/r_*$, can lie only in the interval $1 > x_1 \geqslant x_0$, where $x_1 = x_0 = \approx 0.755$ corresponds to the case of a source with $w(x_0) = 0$, $t(x_0) = 0$, i.e., to the acceleration and heating (by virtue of the current flow) of an initially cold plasma at rest. Any other (nonvanishing) values $w(x_1)$, $t(x_1)$ on the surface of the source must be found from the solution derived (Fig. 1). The relative position of the surface of the source, $x_1 = r_1/r_*$, and of the critical point will also be determined by the solution shown in Fig. 1.

Knowing the behavior $w(x)$, $t(x)$ from Eq. (8), on whose left side we discard the last terms, we can find the potential distribution [$\varphi_0 = \varphi(x_0)$]:

$$\varphi(x) - \varphi_0 = \frac{5}{6\varepsilon}\left(\frac{w}{\gamma} + 3t\right) + \alpha_T. \tag{15}$$

This distribution is shown for various values of γ and Z_i [since we have $\alpha_T = \alpha_T(Z_i)$] in Fig. 2. We see that the potential distribution depends strongly on the value of γ, in contrast with the behavior $w(x)$, $t(x)$.

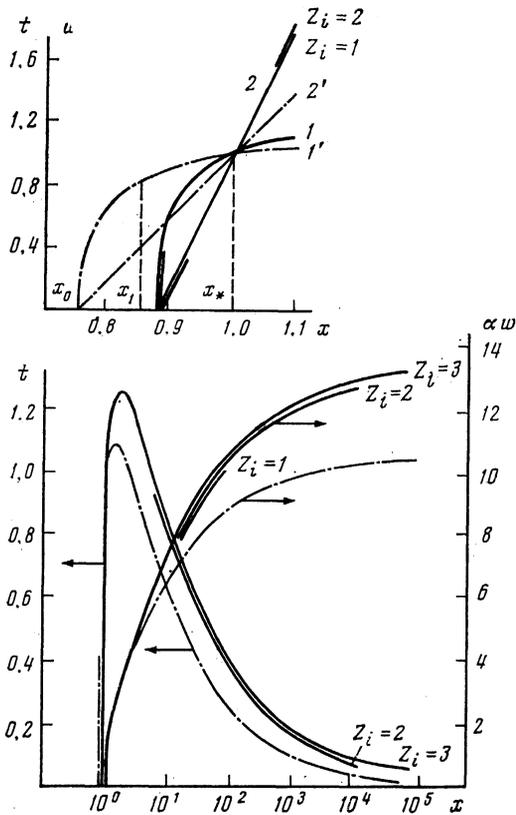Knowing the characteristic flow parameter, $\beta = 5$, we

FIG. 1. Profiles of the electron temperature (1,1') and the ion energy (2,2') along a plasma jet. Solid lines—Results of calculations with a thermal conductivity ($\alpha = 1/2$, $\gamma = 10$, $Z_i = 1,2,3$); dot-dashed lines—results of calculations without a thermal conductivity ($\alpha = 5/6$).

can evaluate the validity of the two basic assumptions which we used in solving this problem. Since the parameter appears in the combination $\varepsilon_x \varepsilon^2/\beta$ (where $\varepsilon_x \approx 2$) in the heat flux in Eq. (8), the quantity $\varepsilon = 1 - \gamma^{-1}$ must be sufficiently small if we are to ignore the thermal conductivity. This condition is satisfied at about $\gamma < 2$. The latter inequality can also be thought of as the condition under which the thermal conductivity has only a slight effect on the expansion of a current-carrying plasma.

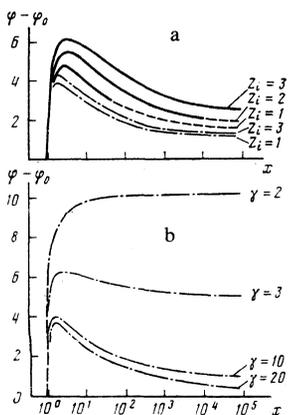We can also evaluate the validity of the hydrodynamic

FIG. 2. Potential profile along a plasma jet with (solid lines) and without (dot-dashed lines) a thermal conductivity. a—$\gamma = 10$, $Z_i = 1$-3; b—$\gamma = 2$-20, $Z_i = 1$.

approximation [i.e., the validity of our initial equations, (1)-(5)]. The validity of this approximation is not obvious, since as the plasma expands into vacuum it ultimately becomes collisionless. Working from (9) and the data in Fig. 1, we find the estimate $Kn(x) \approx Kn_* x \approx (m_e/m_i)^{1/2} x$, from which it follows that the hydrodynamic description of the plasma is valid to $x < (m_i/m_e)^{1/2}$.

3. EFFECT OF THERMAL CONDUCTIVITY ON THE PLASMA EXPANSION

We now consider the spherical expansion of a plasma with thermal conductivity. In other words, we turn to the solution of the complete system of equations in (6)-(8) with $s = x^2$. With the critical point again at $x = 1$ (i.e., $r = r_*$), we work from the condition that the sound velocity is crossed to find $\alpha = 1/2$ and

$$\left[\frac{\alpha}{\gamma} + \frac{5}{2} + (\alpha_T - 1)\varepsilon - h\right]\frac{\beta}{\varepsilon_x \varepsilon^2} = 2,$$

from which we can determine the constant h. As a result, the system of equations to be solved becomes

$$\frac{dw}{dx} = \frac{t}{x}\frac{1-F/2xt^{1/2}}{1-t/w}, \tag{16}$$

$$\frac{dt}{dx} = \frac{F}{x^2 t^{5/2}}, \tag{17}$$

$$\frac{d\varphi}{dx} = \frac{\beta}{\varepsilon x^2 t^{1/2}} + \frac{\alpha_T F}{x^2 t^{5/2}} - \frac{1}{2}\frac{dw}{dx}, \tag{18}$$

where

$$F(w,t,\varphi)$$
$$= 2 + \frac{\beta}{\varepsilon_x \varepsilon^2}\left[\frac{1}{2\gamma}(w-1) + \left(\frac{5}{2} + \alpha_T \varepsilon\right)(t-1) - \varepsilon(\varphi-1)\right]. \tag{19}$$

From this system we can easily find the derivative dw/dx at the critical point [this value of the derivative is not determined by Eq. (16) alone]:

$$w_*' = \frac{1}{2}\{2-\zeta+[(2-\zeta)^2+8(16-\zeta(5-\beta))]^{1/2}\}. \tag{20}$$

where $\zeta = \beta/\varepsilon_x \varepsilon^2$. It can be seen from (16)-(20) that the solution of the system depends on the characteristic flow parameter β [defined by (9)], which is still an unknown, in contrast with the case of the expansion of a non-heat-conducting plasma.

A numerical solution of system (16)-(18) has shown, however, that for an arbitrary value of β one finds solutions with a temperature which either rises at large values of x or drops rapidly to zero. The solution which corresponds to the formulation of the problem of expansion into vacuum ($T_e \to 0$ as $x \to 0$) runs along the line separating these two groups of solutions and is found at a strictly determined value of β, which is a unique value for given values of Z_i and γ. Figure 3 shows a curve of $\beta(\gamma)$ found numerically for $Z_i = 1$-3. We see that at small values of γ the $\beta(\gamma)$ curve approaches the value $\beta = 5$, found for a non-heat-conducting plasma, while at large values of γ it reaches values about twice as high.

Figures 1 and 2 show distributions of the temperature, the energy, and the potential calculated for $\gamma = 10$. We see that, as in the case of a non-heat-conducting plasma,
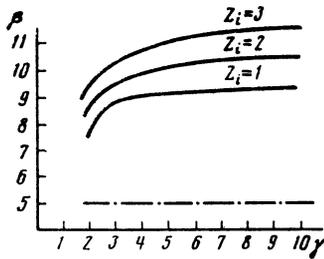
FIG. 3. The characteristic flow parameter β versus the ratio of the electron and ion currents, γ, with (solid lines) and without (dot-dashed line) a thermal conductivity.

$t(x)$ and $w(x)$ depend slightly on Z_i (and also on γ, as the calculations show). This fact was utilized for an approximate calculation of the potential $\varphi(x)$ for $Z_i = 1$ and 2 at large values of x (the dashed continuation of the solid line in Fig. 2), in which case the numerical calculations are not accurate enough to reveal the line separating the rising and sharply falling solutions $t(x)$. For the value $Z_i = 3$, it was found possible to identify this line (i.e., the supersonic solution being sought), up to $x = 10^5$.

A comparison of the solutions with and without thermal conductivity (Fig. 1) shows that the relative changes in the ion energy agree well (at $x > 3$) if the normalization $W_i/Z_i T_* = \alpha w(x)$ is used, but they do not agree well when a normalization to the energy of the critical point, $W_i/W_* = w(x)$, is used. The relative changes in the temperature $t(x)$ are not greatly different in the initial region (after the critical point is passed), while at large values of x the thermal conductivity maintains the electron temperature at a higher level. The ratio of the radius of the spherical source to the position of the critical point, $x_0 = r_0/r_*$, increases to $x_0 \approx 0.88$ when the thermal conductivity is taken into account (Fig. 1). In other words, the critical point approaches the surface of the sphere.

The thermal conductivity has an important effect on the potential difference $\varphi(x) - \varphi_0$. While in the absence of a thermal conductivity there is essentially no dependence on the ion charge Z_i [since this potential difference is due exclusively to the weak dependence $\alpha_T(Z_i)$ according to (15)], in the case at hand we find a well-expressed increase in the potential with increasing Z_i. It turns out that this potential increase stems from the appearance of an oppositely directed heat flux from the expanding plasma toward the surface of the source. A calculation shows that, although t vanishes as $x \to x_0$ (Fig. 1), its derivative blows up ($dt/dx \to \infty$), and the relative heat flux to the sphere,

$$q = \frac{x^2 t^{5/2}}{\zeta} \frac{dt}{dx},$$

remains nonzero, increasing rapidly with increasing Z_i. Specifically, for the values $Z_i = 1$, 2, and 3, this relative heat flux has the values 0.01, 0.17, and 0.60, respectively. The thermal conductivity thus removes some of the Joule-heating energy from the plasma jet, with the result that a greater potential drop is required in order to maintain a given current in the expanding plasma.

4. DISCUSSION OF THE RESULTS OF THE CALCULATIONS

This study shows that during the steady-state flow of a current-carrying ($\gamma > 1$) plasma away from the surface of a sphere of arbitrary radius the plasma is heated and accelerated to supersonic velocities over a distance $\Delta r = r_* - r_0 \approx 0.1 r_0$, near the surface of the sphere. A maximum appears (at $r \approx 2r_0$) on the temperature distribution as a result of the Joule heating of the initially cold and very dense plasma ($T_e \to 0$ and $N_e \to \infty$ as $r \to r_0$) and the subsequent cooling of this plasma due to the expansion ($T_e \to 0$ and $N_e \to 0$ as $r \to \infty$). The potential distribution for $\gamma > 2$ also has a maximum, which lies near the temperature maximum and shifts to slightly greater distances as Z_i is increased and γ reduced (Fig. 2). This shift is accompanied by a decrease in the negative potential gradient and an increase in the overall voltage drop along the jet, $\varphi_\infty - \varphi_0$. In the opposite case of large values of γ, the peak in the potential distribution $\varphi(x)$ becomes sharper, and the overall voltage drop $\varphi_\infty - \varphi_0$ decreases, approaching zero as $\gamma \to \infty$. The physical reason for this effect is clear: At a low ion current $I_i \ll I_e$, the electron energy expended on accelerating ions decreases sharply.

The positive potential gradient depends weakly on Z_i and γ and is realized in the interval $3r_0 > r > r_0$, which is also the interval in which the plasma is rapidly heated and accelerated. Electrons are accelerated in this case by both the intrinsic pressure and the electric field, while the ions (moving opposite the field) are accelerated by the friction force

$$\mathbf{R}_{ie} = -eN_e \mathbf{j}/\sigma$$

(an entrainment by the "electron wind" or "ohmic" acceleration).[19] This force remains predominant out to distance $r \lesssim 10^2 r_0$ (over which most of the acceleration occurs, as can be seen from Fig. 1). The electric field then assumes the leading role in the acceleration (the region of a negative potential gradient). The relative increase in the ion energy in this region, however, is fairly small. For the plasma jet as a whole (in view of its quasineutrality), we can say that the jet is accelerated by the gradient of the electron pressure which is maintained by Joule heating, itself a result of the current flow.

As was shown in the preceding sections of this paper, a supersonic expansion of a current-carrying plasma of a current-carrying plasma is possible at only a single value of the characteristic flow parameter β, which is a single-valued function of the ion charge Z_i and the current ratio $\gamma = I_e/I_i$ (Fig. 3). The spatial distributions of the dimensionless hydrodynamic properties of the plasma, $w(t)$, $t(x)$, and $n(x)$ and that of the potential $\varphi(x)$ also depend on Z_i and γ alone. This dependence is very weak in the cases of w, t, and n. To find the distributions of the absolute values, $W_i(r)$, $T_e(r)$, $N_i(r)$, and $\Phi(r)$, we need to also specify the current $I = I_e - I_i$ and the radius of the sphere from which the plasma is emerging, r_0. Specifically, if we take account of the dependence $\sigma(T_e)$ and assume $\delta \approx 1$ and $r_0/r_* \approx 0.9$, we find from (9)

$$T_e^{3/2} = C \frac{\varepsilon Z_i I}{\beta r_0 \Omega}, \tag{21}$$

where $C \approx 3.75 \cdot 10^{-2}$ eV$^{5/2}$ cm/A, $\varepsilon = 1 - \gamma^{-1}$,

$\beta = \beta(\gamma, Z_i)$ (Fig. 3), and Ω is the solid angle in which the current I is flowing. Since all the other dimensional quantities can be expressed in terms of T_* and the dimensionless solutions $w(t), t(x), \varphi(x)$, we see that all the characteristics of the current-carrying plasma during its spherical supersonic expansion are determined unambiguously by a specification of the integral currents I_e and I_i (or I and γ), the sphere radius r_0, and the parameters Z_i and m_i of the plasma particles. It is not necessary to specify boundary conditions, i.e., local values of the hydrodynamic parameters of the plasma (N_i, W_i, T_e), at the surface of the sphere.

5. APPLICATION OF THE THEORY OF SPHERICAL EXPANSION OF A PLASMA TO VACUUM ARCS

5.1. General characteristics of arcs

Let us use the solution which has been found to analyze experimental data on the vacuum arc, which is an electric discharge in an evacuated gap between electrodes. This analysis is convenient since the plasma in such systems propagates away from the cathode (the cathode material is the material from which the plasma is produced) toward the anode in the form of a quasisteady, expanding, current-carrying jet. In addition, many years of research on vacuum arcs have provided us with extensive experimental data, which have not previously been analyzed as a whole from a common standpoint.

The plasma jet in a arc flows out of local regions near the surface of the cathode: cathode spots. Arcs are put in two categories on the basis of the characteristic dimension (diameter) of these spots. The first category is that of arcs with a contracted spot, with $a \approx 10^{-3} - 10^{-2}$ cm (Ref. 8 and 20), and the second is that of arcs with a diffuse spot, with $a \approx 10^{-1} - 10^0$ cm (Refs. 14 and 21). The experimental data support the suggestion that when the source of plasma in a contracted-spot arc is a single spot (this case is observed at $I < I_{max}$, where I_{max} depends on the cathode material) the spot diameter is proportional to the current: $I/a \approx \text{const} \approx 10^4$ A/cm (Refs. 20 and 22).

In order to apply the theoretical results to vacuum arcs, we need the radius (r_0) of the sphere from which the plasma is merging, the solid angle Ω (in which the current $I = I_e - I_i$ is flowing), the ratio of electron and ion fluxes ($\gamma - I_e/I_i$), and the ion charge Z_i.

According to the measurements, the plasma jet of a contracted-spot arc has an angular size $\theta_0 \approx 30°$ (Refs. 7, 15, and 23). From this figure we find an angle $\Omega = 2\pi(1 - \cos\theta_0) \approx 1$. Approximately the same values are found for diffuse-spot arcs.[14] In this case the assumption $r_0 \approx a$ is fairly accurate.

Measurements have shown[20,24] that for a contracted-spot arc the ratio of electron and ion currents, $\gamma = 10-12$, is essentially a constant, independent of the size of the electrodes, the distance between the electrodes, the current ($I = 50-1000$ A), and the properties of the cathode material. For diffuse-spot arcs without special cathode heating, this ratio again is approximately a constant ($\gamma = 9-20$; Ref. 21), while with deliberate heating we find $\gamma \approx 8-30$ (under the assumption $Z_i = 3$).[14] In all the calculations below we use the value $\gamma = 10$.

In comparing the theoretical results (calculated for a plasma with a single ion species) with experimental data, we use as the ion charge Z_i its average value $\overline{Z}_i$. In a contracted-spot arc, this average value has been measured for various cathode materials. The results reported by different investigators usually agree within 10% (Refs. 7, 20, 25, and 26). Corresponding values of $\overline{Z}_i$ are shown in Table I. No direct measurements of Z_i are available for diffuse-spot arcs; all that is known is that these values are smaller than for contracted-spot arcs.[8,28]

5.2. Theoretical expressions for a vacuum arc

Using the typical value $\gamma \approx 10$ (and thus $\beta \approx 10$ and $\varepsilon \approx 0.9$) and $\Omega \approx 1$, we find from (1) and (21)

$$T_e(r) = fZ_i^{2/5}t(x), \quad W_i(r) = fZ_i^{7/5}w(x)/2, \tag{22}$$

$$N_i(r) = \frac{C_1\mu_i^{1/2}}{Z_i^{1.7}f^{1/2}} \frac{I}{r^2[w(x)]^{1/2}}, \tag{23}$$

where

$$f = C_0(I/a)^{2/5}. \tag{24}$$

Here $C_0 = 0.1$ eV$\cdot$cm$^{2/5}$/A$^{2/5}$, $C_1 = 7\cdot10^{11}$ eV$^{1/2}$/(A$\cdot$cm), μ_i is the ion mass in atomic mass units, $r = z + a$, $x = z/a + 1$, and z is the distance from the surface of the cathode along the axis of the plasma jet. Since the vast majority of measurements in vacuum arcs are carried out at distances $z \gtrsim 1$ cm, for contracted-spot arcs ($a \approx 10^{-2}$ cm) we have $r \approx z$, $x \approx z/a \gtrsim 10^2$ and $w(x) \approx 20$, $t(x) \lesssim 0.3$. For diffuse spot arcs ($a \approx 1$ cm) we have $x \approx 2-10$ and $t(x) \approx 1$.

The overall voltage drop in the arc is determined by the equation

$$eU = fZ_i^{2/5}\Delta\varphi, \quad \Delta\varphi = \varphi(x_l) - \varphi_0, \tag{25}$$

where $x_l = l/a + 1$, and l is the distance between electrodes.

To calculate the properties of the arc we need data on the size of the cathode spot, $a(I)$, as can be seen from (22)–(25). If we use the experimental estimate above, and if we assume that the ratio $I/a \approx 10^4$ A/cm is approximately con-

TABLE I. Average ion charge in vacuum arcs with various cathode materials.

Element	Zn	Cd	C	Ag	Ca	Mg	Al	Ni
$\overline{Z}_i$ Reference	1 [20]	1 [7 20]	1 [25]	1.4 [25]	1.5 [25]	1.5 [25]	1.5 [7, 25]	1,5 [7, 25]

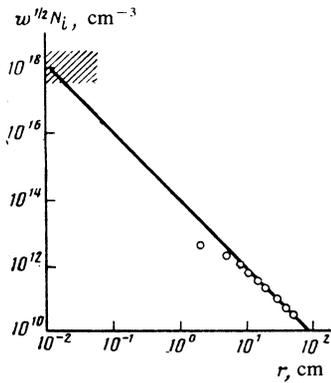| Element	Fe	Cu	Ti	Cr	Zr	Ta	Mo	
$\overline{Z}_i$ Reference	1,5 [20, 26]	1.8 [20, 25, 26]	1.8 [26]	2,0 [26]	2.2 [25]	2.7 [25]	2,0 [25]	2,9 [26]

FIG. 4. Profile of the ion density (at $I \approx 100$ A) along the arc axis. Hatched region—Data of Ref. 8; points—data of Ref. 9; line—expression (23) ($w^{1/2}N_i \propto r^{-2}$).

stant, we find $f \approx 4$ eV from (24). In the discussion below, however, we will not postulate a value of f at the outset; we will instead find it from an analysis of the fairly diverse experimental data (ion energies, ion density distributions, and the overall voltage drops across the arcs).

5.3. Density distribution

Direct measurements of the electron density far from the cathode by probes[9,18] and also near a cathode spot in a contracted-spot arc by spectroscopic methods[8] have made it possible to construct spatial profiles of the normalized flux density, $w^{1/2}N_i(r)$ (Fig. 4). The results of these measurements can be approximated satisfactorily by a power law $w^{1/2}N_i \propto r^{-2}$. From the proportionality factor in this law and from (23) we find $f \approx 4.6$ eV (for $Z_i \approx 1.8$, $I = 100$ A, and $\mu_i \approx 50$). From (24) we then find the radius of the sphere which is the plasma source: $r_0 \approx a \approx 0.7 \cdot 10^{-2}$ cm.

5.4. Energy of the ions

Figure 5 shows values of the directed energy of the ion fluxes in contracted-spot arcs with various values of the average charge $\bar{Z}_i$, taken from the most detailed measurements of the ion energy distributions with separation by charge.[25,26] According to (22) and (24), the slope of the straight line approximating the experimental results in Fig. 5 yields $f \approx 4.0$ eV. From this value and the known current $I = 100$ A, we find the radius of the source surface to be $r_0 \approx a \approx 10^{-2}$ cm (here $w \approx 20$ cm; see Fig. 1).
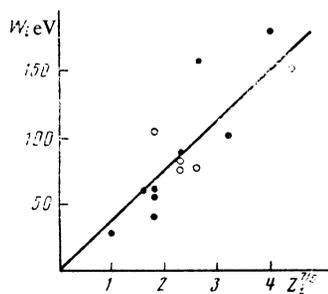

FIG. 5. Average ion energy (at $x \approx 10^2$–10^5 and $I = 100$ A) versus the average ion charge. ●—According to data of Ref. 25; ○—according to data of Ref. 26.

For the most part, the data in Fig. 5 [in particular, the values W_i(Mo) ≈ 150 eV, and W_i(Ti) ≈ 70 eV] were found at large distances from the cathode: $r \gtrsim 50$ cm. The ion energy distributions measured with grid probes (without separation by charge) at smaller distances yield substantially smaller values of W_i; at $r \approx 25$ cm, for example, we have values W_i(Mo) $\lesssim 30$–60 eV (Ref. 23), and at $r \approx 20$ cm we have W_i(Mo) $\lesssim 30$ eV (Ref. 18). A similar conclusion regarding arcs with cathodes of other metals (Al, Ag, Ni, Cu) follows from a comparison of the results of Ref. 7 with those of Refs. 25 and 26.

Direct measurements of the ion energy distributions at various distances from the cathode carried out with the help of a movable grid probe in a contracted-spot arc[18] have revealed a substantial increase in the directed energy of titanium ions, $\Delta W_i \approx 45$ eV, between $r = 15$ cm and $r = 40$ cm. In this region, the acceleration mechanism described in the present paper is no longer effective (Fig. 1). The circumstance allowed Borzenko et al.[18] to suggest an anomalous, turbulent nature of the electron-ion friction force in (4), which is responsible for a transfer of momentum from electrons to ions in this interval. Further evidence in favor of this suggestion comes from measurements in Refs. 9 and 18 of the potential profile $\varphi(x)$, which turned out to be a growing profile, in contrast with the theoretical predictions. The measured increase in the potential, $\delta\varphi \approx 4$ eV (Ref. 9) (or $\delta\varphi \lesssim$ eV in Ref. 18) would lead to an ion-energy increase ΔW_i(Mo) $\approx Z_i\gamma\delta\varphi \approx 80$ eV (Ref. 11) [ΔW_i(Ti) $\lesssim 20$ eV], in reasonable agreement with the results reported.

5.5. Potential profile

The potential distribution in the gap of a vacuum arc is still under discussion. In an effort to explain the fast-ion fluxes seen experimentally, Plyutto et al.[7] suggested that there is a potential maximum ("hill") near the cathode and that beyond this maximum, i.e., in a region of a field which accelerates ions, atoms generated by the cathode are ionized. In Ref. 11, in contrast, the potential profile was assumed to be a monotonically increasing profile, and the ion acceleration was linked with an entrainment of the ions by a stream of electrons moving in an accelerating field from the cathode to the anode.

The results of numerical calculations on the plasma flow in a vacuum arc reveal a potential hill for certain specific values of the flow parameters.[12,14] The conditions for the existence of this hill, the dependence of the height of the hill on the flow parameters, and the role played by this hill in the ion acceleration process, however, were not explained. The potential profiles in Fig. 2(b) show that a hill appears even at small values of the parameter showing the extent to which the flow is of a "current" nature: $\gamma > \gamma_{thr} \approx 2$. The height of this hill, $\varphi_{max} - \varphi_\infty \approx \varphi_{max} - \varphi(x \approx 10^5)$, increases with increasing γ. The potential hill is thus a characteristic feature of specifically systems which are of a current nature.

Figure 2 also shows that the potential reaches a maximum at $x = x_m \lesssim 2$. In the case of a contracted-spot arc ($r_0 \lesssim 10^{-2}$ cm), this result corresponds to a distance $r_m = x_m r_0 \lesssim 2 \cdot 10^{-2}$ cm from the cathode, and it would be essentially impossible to observe a hill in this case. For diffuse-spot arcs ($r_0 \gtrsim 1$ cm) the value of r_m can reach several centimeters and would be quite amenable to measurements.
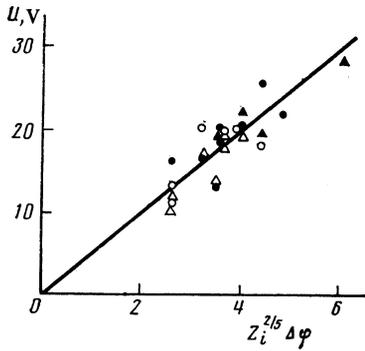
FIG. 6. Total voltage drop across the arc ($I = 100$ A) versus the average ion charge. ●—According to data of Ref. 25; ▲—Ref. 26; ○—Ref. 24; △—Ref. 7.
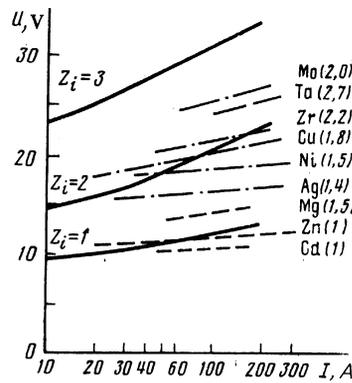

FIG. 7. Current-voltage characteristics of vacuum arcs. Solid lines—Theoretical; dot-dashed lines—data of Ref. 25; dashed lines—data of Ref. 7 (shown in parentheses are the values of $\bar{Z}_i$ for the corresponding cathode material).

In fact, a potential hill has recently been observed experimentally under these conditions.[27]

5.6. Total potential drop across an arc

It follows from Fig. 2(a) that as the gap length in a contracted-spot arc is varied over the wide range $l = 0.5$–50 cm (correspondingly, $x \approx 5 \cdot 10^1$–$5 \cdot 10^3$) the value of $\Delta\varphi$ changes by ~ 30–40%. In other words, the total voltage drop across the arc also depends weakly on the gap length according to (25). This fact has been noted repeatedly in experiments (e.g., Ref. 24).

The quantity U is known for various experimental conditions, i.e., for various cathode materials, arc currents, and gap lengths. Figure 6 shows U in contracted-spot arcs with various cathodes as a function of the parameter $Z_i^{2/5}\Delta\varphi$, where Z_i is also known, for each cathode material, from measurements (Table I), and $\Delta\varphi(Z_i)$ has been calculated [Fig. 2(a)]. It follow from Fig. 6 that a linear law, as in (25), is a satisfactory description of the relationship between these parameters, with a coefficient $f \approx 4.8$ eV. From (24) we then find a source radius $r_0 = a \approx 0.6 \cdot 10^{-2}$ for a current $I \approx 100$ A.

Using this value of f, and assuming that it remains constant as the current is varied, we can find the dependence $U(I)$, i.e., the current-voltage characteristic, for a contracted-spot arc. This behavior arises because the quantity a in-

creases with increasing current under assumption. In other words, the normalized gap length l/a decreases. It can be seen from Fig. 2(a) that the value of $\Delta\varphi$, i.e., U, increases. Figure 7 shows experimental current-voltage characteristics of contracted-spot arcs for various cathode materials, along with theoretical characteristics for arcs with various ion charges. It can be seen from Fig. 7 that (first) the behavior of the theoretical characteristics is similar to that of the experimental characteristics; specifically, there is a slight increase in $U(I)$. Second, the values of U are themselves approximately the same for materials with various Z_i. The value of U increases with increasing Z_i. Third, there is a sharper rise of the $U(I)$ curve for materials with large Z_i, both theoretically and experimentally. We might add that the last two of these effects arise in the calculations specifically because a thermal conductivity was taken into account [Fig. 2(a); this conductivity also leads to a fairly strong dependence of $\Delta\varphi$ on Z_i] in order to reconcile the theoretical results with the experimental results.

5.7. Electron temperature

Table II summarizes the results of the measurements and calculations of T_e in a contracted-spot arc. We see from this table that the theoretical values (T_e^T) and the experi-

TABLE II.

Cathode material	$\bar{Z}_i$	$x = r/r_0$	$T_e^{(T)}$, eV	$T_e^{(E)}$, eV	Method for measuring T_e; reference
Cu Mg Ni Ag	1,8	~ 1	6	6–10	From charge composition of ions; Ref. 7
Zn Cd Pb $\}$	1	~ 1	4	3–4	From charge composition of ions; Ref. 7
Cu	1,8	~ 1	6	2	From relative intensity of Cu^{2+} spectral line; Ref. 8
Mo	2,0 (2,9)	$\sim 10^3$	0,8 (1,0)	3	Langmuir probe; Ref. 23
Ti	1,8	$\sim (1 \div 3) \cdot 10^3$	0,8–0,6	1,2–1,5	Langmuir probe; Ref. 9

mental values (T_e^E) agree fairly well near a cathode spot, with similar tendencies to increase with increasing Z_i, in accordance with (22). With distance from the cathode we see a decrease in the temperature in both cases, but $T_e^E(r)$ decreases considerably more slowly than $T_e^T(r)$, possibly because of the turbulence effect mentioned above. That effect would lead to anomalously low values of the conductivity and thus to a power level of the Joule heating of electrons higher than that found in the calculations.

5.8. Distinctive features of diffuse-spot arcs

Working from these results, we can offer a qualitative explanation for certain trends which have been observed experimentally in the transition from contracted-spot to diffuse-spot arcs.[21,28] This transition corresponds to an increase in the size of a cathode spot by one or two orders of magnitude. The normalized coordinate $x = r/r_0$ decreases by the same factor (i.e., the arc becomes "short"). In addition, the value of the factor f in (22)–(24) decreases by a factor of three to ten. It follows that this transition should be accompanied by a decrease in the total voltage drop across the arc; this conclusion corresponds to experimental data of Ref. 21. Furthermore, according to (22) and Fig. 1 there will be decreases in the directed energy and the temperature of the electrons, so the average ion charge, $\overline{Z}_i$, which is determined by T_e, will also decrease. These effects have also been seen experimentally.[28] The ratio $U/T_e = \Delta\varphi/t$ [see (22) and (25)] depend on only Z_i (and then only weakly), and for the experimental conditions of Ref. 14 we would have $U/T_e \approx 4$–5 according to the calculations, while the measurements yield $U/T_e \approx 2.5$–5, while the quantities themselves vary by a factor ~ 6. Finally, the experimental values of the electron temperature and density near a cathode spot are also close to the values found theoretically: $T_e^{(T)} \approx 1$ eV, $N_e^{(T)} \approx (2$–$10) \cdot 10^{13}$ cm^{-3}, $T_e^{(E)} \approx 2$–4 eV, $N_e^{(E)} \approx (1$–$3) \cdot 10^{13}$ cm^{-3} (Refs. 14 and 21).

5.9. Estimate of the effect of the magnetic field

Since the plasma does not flow out from the entire surface of the sphere in the case of a vacuum arc, but only from some solid angle $\Omega = 2\pi(1 - \cos\theta_0)$, the current flowing in the plasma creates an axisymmetric magnetic field $B(r,\theta)$. To estimate the effect of this field on the plasma outflow, we ignore (as above) the variation of the plasma parameters across the plasma cone $\theta \leqslant \theta_0$. The magnetic field at $\theta \leqslant \theta_0$ is then given by

$$B(r,\theta) = \frac{4\pi I}{c\Omega r} \frac{1 - \cos\theta}{\sin\theta}.$$

Using (1) and (21), we can derive an expression for the parameter $\beta_p = p_e/p_B$, the ratio of the gas pressure $p_e = N_e T_e$ to the magnetic pressure $p_B = B^2/8\pi$ and a measure of the effect of the magnetic field:

$$\beta_p(r,\theta) = \frac{I_0}{I} \frac{t(x)}{[w(x)]^{1/2}} \left(\frac{\sin\theta}{1 - \cos\theta}\right)^2,$$

$$I_0 = \frac{k\mu_i^{0.5}}{\gamma Z_i^{0.3}} \left(\frac{I}{\beta r_0}\right)^{1/5} \left(\frac{\Omega}{\varepsilon}\right)^{1/5}, \qquad (26)$$

where $k \approx 10^2$ A$^{4/5}$ cm$^{1/5}$. For the typical parameter values of a vacuum arc ($\Omega/\varepsilon \approx 1$, $\mu_i^{0.5}/Z_i^{0.3} \approx 5 - 10$, $I/r_0 \approx 10^4$

A/cm, $\gamma \approx \beta \approx 10$) the quantity I_0 lies in a narrow interval and has values close to $I_0 \approx 300$ A.

Let us estimate the ratio β_p at the edge of the cone ($\theta = \theta_0$), where the magnetic field is at its strongest. Assuming $\theta_0 \approx 30°$, we find from (26)

$$\beta_p \approx \frac{3000}{I} \frac{t(x)}{[w(x)]^{1/2}}.$$

(I is the current in amperes). We thus see that in the critical cross section ($x = t = w = 1$) we would have $\beta_p \gtrsim 3$ at currents $I \lesssim 10^3$ A, and we could ignore the effect of the magnetic field. At distances $r \approx 1$ cm from the cathode ($x \approx 10^2$, $t \approx 1$, $w^{1/2} \approx 5$) we find $\beta_p \approx 600/I$; at $r \gtrsim 10$ cm ($x \gtrsim 10^3$, $t \lesssim 10^{-1}$, $w^{1/2} \approx 5$) we find $\beta_p \lesssim 60/I$. The last of these estimates agrees with experimental data[23] at $r = 30$ cm. These data are evidence that the self-magnetic field begins to have an effect at currents $I \gtrsim 100$ A.

Calculations show (Fig. 1) that we have $t(x)/[w(x)]^{1/2} \to 0$ (and thus $\beta_p \to 0$) as $x \to x_0$ and $x \to \infty$. This result means that the magnetic pressure begins to exceed the gas pressure at both large and small distances from the cathode. It may be that by incorporating the effect of the magnetic field near the cathode we would be able to calculate the angular size of the jet, θ_0, and the size of the cathode spot, $a \approx r_0$, which we have been treating as given parameters.

If we assume that a pinch effect is caused in the plasma jet by the self-magnetic field at $\beta_p < 1$, then by setting $\beta_p = 1$ we could determine the boundary surface of the jet, $\theta_b = \theta_b(r)$, from (26). For the typical current value $I \approx 10^2$ A at $x \lesssim 10^2$, this surface would be conical, with $\theta_b \approx \theta_0 = $ const (in agreement with measurements[24] at $r \lesssim 2$ cm), while at large distances the jet would occupy only part of the original cone; i.e., we would have $\theta_b(r) < \theta_0$.

We can draw some conclusions from this analysis. First, incorporating the magnetic field has no significant effect on the basic relations, (21)–(24), since they were derived from the conditions for crossing of the critical point, at which the inequality $\beta_p \gg 1$ holds quite well at $I \lesssim 10^3$ A. Second, the self-magnetic field should lead to a pinch effect in the plasma jet both with increasing distance from the cathode and in the immediate vicinity of a cathode spot. Third, the shape of the plasma jet can be estimated by equating the gas pressure to the magnetic pressure.

CONCLUSION

This study has shown that the supersonic expansion of a plasma is controlled completely by the (integral) initial parameters, and it is not necessary to specify boundary conditions at the surface of the source. Incorporating thermal conductivity leads to (first) the appearance of a heat flux toward the cathode, which intensifies rapidly with increasing ion charge, and (second) a significant dependence of the potential profile on the ion charge.

Our application of this theory of the spherical expansion of a current-carrying plasma to vacuum arcs has made it possible to tie together many pieces of experimental evidence, on the basis of essentially nothing more than the requirements of hydrodynamics, without consideration of effects occurring at the electrode surface. In particular, the source radii found by comparing the theoretical results with these groups of independent experimental data (on the ion

energy, the density distribution, and the total voltage drop across the arc) turn out to agree well with each other and also with experimental estimates of the size of the cathode spot. In this model, the problem of determining the spot size and the ion charge (these properties have been treated as given parameters here) as functions of the cathode material thus remains a problem of analyzing the thermal and electrical processes which occur at the cathode surface and also the elementary processes which occur in the plasma of a cathode spot.

[1] E. N. Parker, Space Sci. Rev. **4**, 666 (1965).

[2] G. N. Abramovich, *Applied Gas Dynamics*, Nauka, Moscow, 1969.

[3] I. I. Litvinov, Zh. Prikl. Mekh. Tekh. Fiz. No. 6, 10 (1971).

[4] A. V. Gurevich, L. V. Pariĭskaya and L. P. Pitaevskiĭ, Zh. Eksp. Teor. Fiz. **49**, 647 (1965) [Sov. Phys. JETP **22**, 449 (1966)].

[5] A. V. Gurevich and A. P. Meshcherkin, Zh. Eksp. Teor. Fiz. **80**, 1810 (1981) [Sov. Phys. JETP **53**, 937 (1981)].

[6] Ch. Sack and H. Schamel, Phys. Rep. **156**, 311 (1987).

[7] A. A. Plyutto, V. N. Ryzhkov, and A. T. Kapin, Zh. Eksp. Teor. Fiz. **47**, 494 (1964) [Sov. Phys. JETP **20**, 328 (1965)].

[8] G. A. Lyubimov and V. P. Rakhovskiĭ, Usp. Fiz. Nauk **125**, 665 (1978) [Sov. Phys. Usp. **21**, 693 (1978)].

[9] I. I. Aksenov, I. I. Konovalov, V. B. Padalka, *et al.*, Fiz. Plazmy **11**, 1373 (1985) [Sov. J. Plasma Phys. **11**, 787 (1985)].

[10] M. Lookwood, Adv. Space **6**, 63 (1986).

[11] M. P. Zektser and G. A. Lyubimov, Zh. Tekh. Fiz. **49**, 3 (1979) [Sov. Phys. Tech. Phys. **24**, 1 (1979)].

[12] B. Ya Moĭzhes and V. A. Nemchinskiĭ, Zh. Tekh. Fiz. **50**, 78 (1980) [Sov. Phys. Tech. Phys. **25**, 43 (1980)].

[13] B. A. Uryukov, Izv. SO AN SSSR Ser. Tekhn. No. 2, 34 (1982).

[14] S. Ya. Bronin, V. P. Polishchuk, P. E. Sychev, *et al.*, Preprint 2-199, Institute of High Temperatures, Academy of Sciences of the USSR, Moscow, 1986.

[15] I. I. Beĭlis, M. P. Zektser, and G. A. Lyubimov, Zh. Tekh. Fiz. **58**, 1861 (1988) [Sov. Phys. Tech. Phys. **33**, 1132 (1988)].

[16] S. I. Braginskiĭ, in *Reviews of Plasma Physics, Vol. 1* (ed. M. A. Leontovich), Consultants Bureau, New York (1965).

[17] L. Spitzer, Jr., and R. Härm, Phys. Rev. **89**, 977 (1953).

[18] V. P. Borzenko, O. L. Volkov, V. I. Krasov, *et al.*, Pis'ma Zh. Tekh. Fiz. **14**, 435 (1988) [Sov. Tech. Phys. Lett. **14**, 195 (1988)].

[19] A. I. Morozov and E. V. Artyushkov, *International Symposium on the Properties and Applications of Low-Temperature Plasmas* (Moscow, 1965), Mir, Moscow, 1967.

[20] J. E. Daalder, Physica B + C **104**, 91 (1981).

[21] A. I. Vasin, A. M. Dorodnov, and V. A. Petrosov, Pis'ma Zh. Tekh. Fiz. **5**, 1499 (1979) [Sov. Tech. Phys. Lett. **5**, 634 (1979)].

[22] L. Harris, in *Vacuum Arcs* (ed. J. M. Lafferty), Wiley, New York, 1980 (Russ. Transl. Mir, Moscow, 1982).

[23] V. M. Dunev, V. D. Ovcharenko, and V. M. Khoroshikh, Zh. Tekh. Fiz. **47**, 1486 (1977) [Sov. Phys. Tech. Phys. **22**, 855 (1977)].

[24] C. W. Kimblin, J. Appl. Phys. **44**, 3074 (1973).

[25] W. D. Davis and H. C. Miller, J. Appl. Phys. **40**, 2212 (1969).

[26] V. M. Lunev, V. G. Padalka, and V. M. Khoroshikh, Zh. Tekh. Fiz. **47**, 1491 (1977) [Sov. Phys. Tech. Phys. **22**, 858 (1977)].

[27] S. I. Arestov, S. P. Bugaev, A. N. Sukharev, *et al.*, *Proceedings of the Seventh All-Union Conference on the Physics of Low-Temperature Plasmas*, FAN, Tashkent, 1987, Part 2, p. 93.

[28] I. I. Aksenov, V. G. Bren', I. I. Konovalov, *et al.*, Teplofiz. Vys. Temp. **21**, 646 (1983).

Translated by Dave Parsons

459   Sov. Phys. JETP **70** (3), March 1990

Krinberg *et al.*   459